Chinese Chemical Letters 31 (2020) 751–754

Contents lists available at ScienceDirect

Chinese Chemical Letters

journal homepage: www.elsevier.com/locate/cclet

Communication

Inhibition of the toxic byproduct during photocatalytic NO oxidation *via* La doping in ZnO

Chaowei Yuan[a], Wen Cui[b,c], Yanjuan Sun[a,b,*], Jiadong Wang[a], Ruimin Chen[a], Jin Zhang[a], Yuxin Zhang[d], Fan Dong[a,b,*]

[a] *Chongqing Key Laboratory of Catalysis and New Environmental Materials, College of Environment and Resources, Chongqing Technology and Business University, Chongqing 400067, China*
[b] *Research Center for Environmental Science & Technology, Institute of Fundamental and Frontier Sciences, University of Electronic Science and Technology of China, Chengdu 611731, China*
[c] *The Center of New Energy Materials and Technology, School of Materials Science and Engineering, Southwest Petroleum University, Chengdu 610500, China*
[d] *College of Materials Science and Engineering, Chongqing University, Chongqing 400044, China*

ARTICLE INFO

Article history:
Received 23 July 2019
Received in revised form 15 September 2019
Accepted 17 September 2019
Available online 18 September 2019

Keywords:
Photocatalytic NO oxidation
Toxic byproduct
Reactive oxygen species
ZnO
Cationic vacancie

ABSTRACT

It is of a great challenge to develop semiconductor photocatalysts with potential possibilities to simultaneously enhance photocatalytic efficiency and inhibit generation of toxic intermediates. In this study, we developed a facile method to induce the La doping and cationic vacancie (V_{Zn}) on ZnO for the highly efficient complete NO oxidation. The photocatalytic NO removal efficiency increases from 36.2% to 53.6%. Most importantly, a significant suppressed NO_2 production also has been realized. According to the DFT calculations, ESR spectra and *in situ* FTIR spectra, the introduction of La^{3+} induce the redistribution of charge carriers in La-ZnO, which promote the production of $^{\bullet}O_2^-$ and lead to the formation of V_{Zn} for the formation of $^{\bullet}OH$, contributing to the complete oxidation of NO to nitrate. Besides, the conversion pathway of photocatalytic NO oxidation has been elaborated. This work paves a new way to simultaneously realize the photocatalytic pollutants removal and the inhibition of toxic intermediates generation for efficient and safe air purification.

Nitric oxide (NO) and nitrogen dioxide (NO_2) are jointly referred to as NO_x [1,2]. Artificially derived NO_x, even at very low concentrations (sub-ppm or parts per billion levels), is one of the major contributors to photochemical smog or acid rain and is primarily responsible for respiratory and cardiopulmonary diseases, which has triggered much social concern [3–9]. Conventionally, some absorbents like active carbon and zeolites are applied to pre-concentrate for subsequent selective catalytic reduction (SCR), wet scrubbing, adsorption, biofiltration, or catalytic decomposition for NO removal [10–13]. However, they are not economically feasible for NO removal at a low concentration ppb [14,15]. Semiconductors-based photocatalysis, as a clean and environmentally friendly technology, has received considerable attention in view of its potentiality for environmental remediation [16–23]. However, limited by the photocatalytic efficiency and unfavorable electronic structure, the generation of toxic intermediates like NO_2 is inevitable during photocatalytic NO oxidation on typical photocatalysts [24–29]. Therefore, it is still a great challenge to inhibit the emission of harmful NO_2 and thus realize the complete oxidation of NO to nitrate in the process of photocatalytic NO degradation.

Generally, NO_2 generation in photocatalytic NO oxidation process can be attributed to the presence of one-oxygen reactive species like hole (O^-), which leads to partial oxidation of NO ($NO + O^- \rightarrow NO_2$) [24]. Therefore, it is very important to regulate the formation of active species, especially superoxide radicals ($^{\bullet}O_2^-$), for the complete oxidation of NO ($NO + {}^{\bullet}O_2^- \rightarrow NO_3^-$) [30,31]. Correspondingly, the reduction of O_2 with conduction-band electrons induce the generation of $^{\bullet}O_2^-$ ($O_2 + e^- \rightarrow {}^{\bullet}O_2^-$) [32] and thus the construction of localization center for electrons in photocatalysts is beneficial to facilitate the adsorption and activation of O_2 molecule for the formation of $^{\bullet}O_2^-$.

ZnO is one of the most common and attainable photocatalysts among numerous semiconductors because of its outstanding properties of physical and chemical stability, low cost and non-toxicity [33–36]. However, the photocatalytic efficiency of pure

* Corresponding authors at: Chongqing Key Laboratory of Catalysis and New Environmental Materials, College of Environment and Resources, Chongqing Technology and Business University, Chongqing 400067, China.
E-mail addresses: syhsyj@163.com (Y. Sun), dfctbu@126.com (F. Dong).

https://doi.org/10.1016/j.cclet.2019.09.033
1001-8417/

ZnO is not ideal (Fig S1 in Supporting information) and the generation of toxic intermediates NO_2 during photocatalytic reaction processes has been largely ignored [37–40]. In this study, selective complete oxidation of NO to nitrate over 96.6% has been achieved by the greatly facilitated formation of $^{\bullet}O_2^-$. Surface charge redistribution of ZnO has been achieved by the La doping and the introduction of cationic vacancie (V_{Zn}), accelerating the adsorption and activation of reactants to induce the generation of active radicals for the complete oxidation of NO. Also, highly combined experimental characterization and theoretical simulation show that La doping promote the adsorption and activation of O_2 molecules, resulting in the accelerated formation of $^{\bullet}O_2^-$. Also, the formation of V_{Zn} facilitate H_2O adsorption to produce $^{\bullet}OH$ that processes strong oxidation capacity for photocatalytic NO oxidation. This work develops a novel strategy to regulate the formation of reactive oxygen species for efficient and safe air purification.

Herein, Zinc nitrate hexahydrate ($Zn(NO_3)_2{\cdot}6H_2O$) and lanthanum nitrate hexahydrate ($La(NO_3)_3{\cdot}6H_2O$) were used as zinc and lanthanum sources, respectively. Sodium carbonate anhydrous (Na_2CO_3) were also purchased for the fabrication procedure. All the chemicals were used without any further purification.

La-doped ZnO nanoparticles were prepared by a precipitation method using $Zn(NO_3)_2{\cdot}6H_2O$ and $La(NO_3)_3{\cdot}6H_2O$. Firstly, Zn $(NO_3)_2{\cdot}6H_2O$ and Na_2CO_3 were dissolved separately in double distilled water to obtain 0.5 mol/L solutions. $Zn(NO_3)_2$ solution was slowly added into vigorously stirred sodium carbonate anhydrous solution with the approximate addition rate of around 5 mL/min. Next, $La(NO_3)_3{\cdot}6H_2O$ 0.01 mol/L was slowly added into the above mixture and a white precipitate was obtained. This precipitate was filtered and repeatedly rinsed with distilled water. The resultant solid product was dried at 60 °C for 24 h and calcined in an air oven at 400 °C for 3 h.

As shown in XRD spectra (Fig. 1a), the peaks of pure ZnO at 2θ of 32.11°, 34.75°, 36.59°, 47.85° and 56.93° degree correspond to the (1 0 0), (0 0 2), (1 0 1), (1 0 2) and (1 1 0) planes of hexagonal wurtzite ZnO of the JCPDS No. 36-1451. There are shifts and broadening of XRD characteristic diffraction peaks at $2\theta = 36.59°$ observed, which indicates that La^{3+} ions have been introduced in crystal lattice of ZnO (Fig. 1b). The XPS spectra of O 1s are shown in Fig. 1c. A sharp peak around 530.10 eV can be assigned to the oxygen atoms coordinated with zinc (Zn-O) and the peak at 531.51 eV can be attributed to the La-O [41]. Combined with XRD and XPS results (Fig. S2 in Supporting information), the successful doping of La with ZnO can be demonstrated. Meanwhile, according to EPR spectra (Fig. 1d), two different signals have been detected at g = 1.99 and g = 1.95, corresponding to the vacancy of Zn atom (V_{Zn}) [42] and O atom (V_o) [43], respectively. It's worth noting that new defects (V_{Zn}) appeared in La-ZnO, which is correspond to the lower crystallinity and weaker characteristic diffraction peaks of La-ZnO sample. According to EPR results, the doping of La is in favor of the formation of V_{Zn}, which can be ascribed to the fact that the two La^{3+} replaced three Zn^{2+} for valence equilibrium, resulting in the formation of V_{Zn}.

The SEM and TEM diagrams of ZnO and La-ZnO are shown in Fig. 2. After comparison (Figs. 2a and b), it was found that the morphology of La-ZnO did not change obviously and grain diameter size was around 15–20 nm in both pure and doped ZnO particles. Fig. 2d shows the HRTEM image of the La-ZnO sample, the lattice fringes with a width of 0.244 nm correspond to the (1 0 1) crystal plane of ZnO nanosheets, which is close to the theoretical value of 0.244 nm.

The photocatalytic performance of the prepared samples towards NO removal was evaluated under ultraviolet irradiation (360 nm) as shown in Scheme S1 (Supporting information). As can be seen in Fig. 3a, the photocatalytic NO removal efficiency of pure ZnO is 36.2%, and the removal rate of 3% La-ZnO increases to 53.6%. Apart from a noticeably higher NO removal ratio of 3% La-ZnO, suppressed NO_2 production also have been realized simultaneously, as shown in Fig. 3b. Therefore, efficient and safe NO removal can be achieved by the introduction of La^{3+} and the formation of V_{Zn} on the surface of ZnO to facilitate the complete oxidation of NO to nitrate.

Subsequently, we employ DMPO Spin-trapping ESR Spectroscopy to investigate the formation of $^{\bullet}OH$ and $^{\bullet}O_2^-$ since reactive oxygen species (ROS) are responsible to the oxidation of pollutants

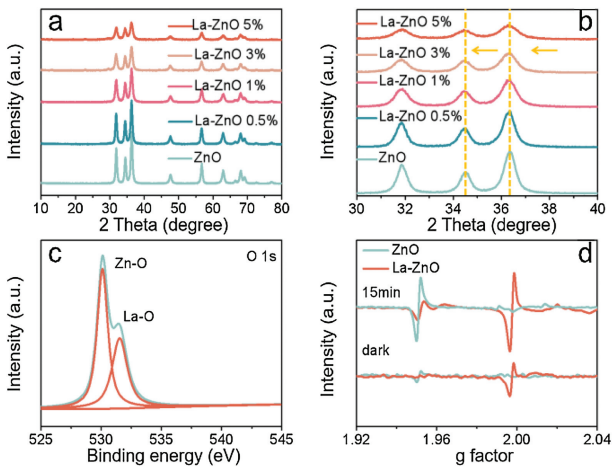

Fig. 1. (a) XRD spectra of pure ZnO and La-ZnO samples; (b) Local enlarged XRD spectra of samples with different La-doped contents ranging from 30° to 40°; (c) XPS spectrum (O 1s) of La-ZnO; (d) EPR spectra of ZnO and La-ZnO.

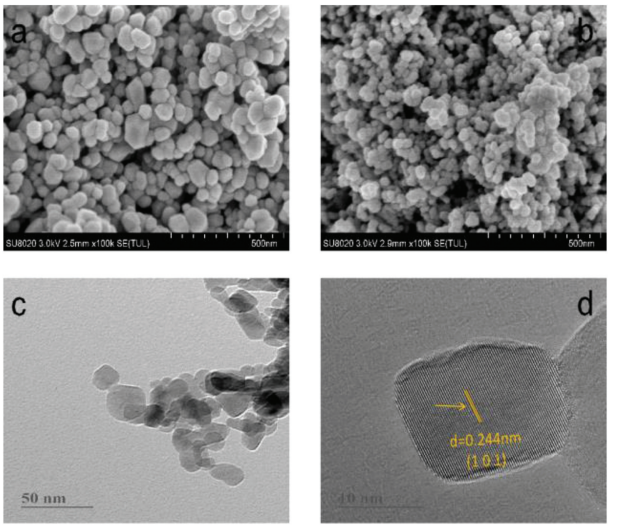

Fig. 2. SEM images for ZnO (a) and La-ZnO (b); TEM (c) and HRTEM (d) images for La-ZnO.

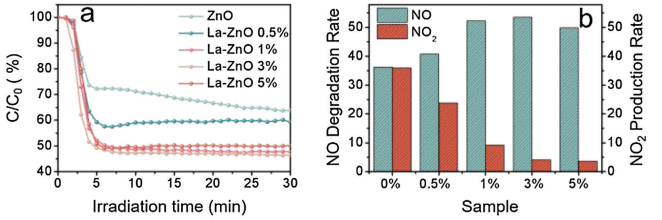

Fig. 3. Photocatalytic activity of pure ZnO and La doped ZnO samples for the removal of NO in air (a) and the comparison of NO degradation rate and NO_2 production rate (b).

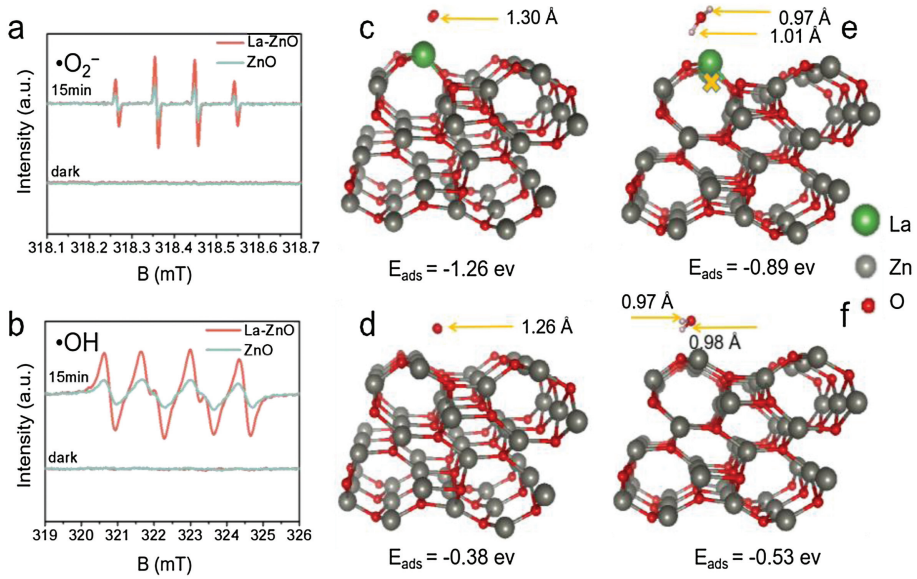

Fig. 4. DMPO ESR spectra in methanol dispersion for $^{\bullet}O_2^-$ (a) and aqueous dispersion for ·OH (b) are carried out in both dark and ultraviolet light irradiation for 15 min, respectively; Optimized local structures of O_2 adsorped La-ZnO (c) and ZnO (d) at surface, respectively; Optimized local structures of H_2O adsorped La-ZnO (e) and ZnO (f) at surface, respectively.

(Reactions 1–6). As shown in Figs. 4a and b, the signals of DMPO-$^{\bullet}O_2^-$ and DMPO-$^{\bullet}$OH of La-ZnO samples are obviously stronger than that of ZnO sample, contributing to the efficient photocatalytic NO removal and suppressed NO_2 generation simultaneously. In addition, the adsorption and activation of O_2 and H_2O molecule were simulated by density functional theory (DFT) calculation to confirm the promoted generation of ROS. Figs. 4c and d display the optimized structure of O_2 adsorption on La-ZnO and ZnO, respectively. The smaller adsorption energy and elongated bond length of O_2 molecules on La-ZnO indicates that O_2 molecule is more easily adsorbed around La atoms and thus more electrons are obtained to form O_2^- for inducing the complete oxidation of NO. Also, H_2O molecule prefer to be adsorbed on V_{Zn} with smaller adsorption energy and elongated bond length on La-ZnO (Figs. 4e and f), giving rise to the activation of H_2O molecule to form $^{\bullet}$OH. Therefore, the introduction of La^{3+} induce the redistribution of charge carriers in La-ZnO, which promote the production of $^{\bullet}O_2^-$ and lead to the formation of V_{Zn} for the formation of $^{\bullet}$OH, contributing to the highly efficient complete oxidation of NO to nitrate.

$$O_2 + e^- \rightarrow {}^{\bullet}O_2^- \quad (1)$$

$$NO + {}^{\bullet}O_2^- \rightarrow NO_3^- \quad (2)$$

$$h^+ + OH^- \rightarrow {}^{\bullet}OH \quad (3)$$

$$NO + {}^{\bullet}OH \rightarrow NO^+ + OH^- \quad (4)$$

$$NO^+ + 2OH^- \rightarrow H_2O + NO_2^- \quad (5)$$

$$NO + 2{}^{\bullet}OH + 2OH^- \rightarrow 2H_2O + NO_3^- \quad (6)$$

Subsequently, the possibility that reactive oxygen species $^{\bullet}O_2^-$ facilitates the complete oxidation of NO to nitrate was further verified by *in situ* diffuse reflectance infrared Fourier transform spectroscopy (DRIFTS) (Scheme S2 in Supporting information). Time-dependent IR spectra during NO adsorption process were dynamically monitored on La-ZnO sample in dark. In the absence of O_2, 100% NO was introduced and subsequently NO adsorption peaks were observed at 1055 cm^{-1} [44] and 1091 cm^{-1} [24] (Fig. 5a). The 1648 cm^{-1} was due to surface undissociated water, as specifically demonstrated by time-dependent *in situ* NO adsorption in the dark [45,46]. Once adsorption equilibrium is achieved, sufficient O_2 was supplied into reaction chamber for 30 min and then ultraviolet light was introduced to trigger photocatalytic reaction. Significant changes of FTIR spectra were vividly observed. During photocatalytic NO oxidation process (Fig. 5b), the peak at 1055 cm^{-1} and 1091 cm^{-1} are gradually decreased and became negative. However, a new absorption band at 1025 cm^{-1} has been found, which is associated with the O—O stretching mode of $^{\bullet}O_2^-$ species [24] and thus contribute to the oxidation of NO to nitrate. Correspondingly, monodentate nitrate with sharp peak at 1254 cm^{-1} and symmetrical surface nitrate with broad peak at 1452 cm^{-1} were detected [47]. The wide band from 1600 to 1800 cm^{-1} was typical of combination band associated with NO and free nitrate [48]. Therefore, the introduction of La^{3+} and the formation of V_{Zn} promote the production of ROS to induce the complete oxidation of NO to nitrate (Fig. 6). After nitrate is accumulated, the catalyst can be regenerated in a simple way by washing it with water [49,50]. Fuller *in situ* DRIFTS spectra on La-ZnO are shown in Fig. S3 (Supporting information). All assignments of the FT-IR bands observed during the adsorption-reaction of NO can be found in Table 1.

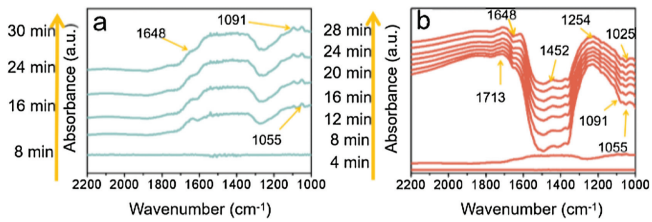

Fig. 5. *In situ* DRIFTS spectra on La-ZnO during NO adsorption process (a) and photocatalytic NO oxidation process (b).

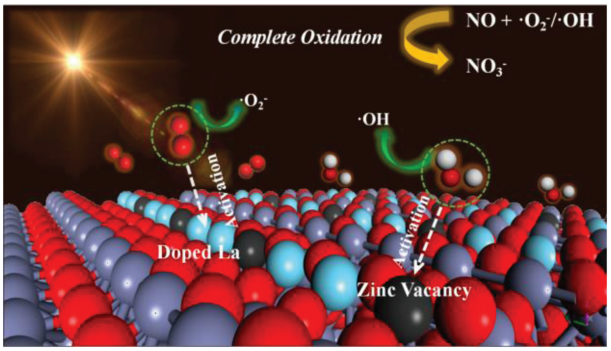

Fig. 6. The illustration of the roles of La-doping and Zinc vacancy in photocatalytic NO oxidation.

Table 1
Assignments of the FT-IR bands observed during the adsorption-reaction of NO on La-ZnO under UV-light irradiation.

Wavenumbers (cm^{-1})	Assignment	Ref.
1025	$^{\bullet}O_2^-$	[24]
1055	NO	[44]
1091	NO	[24]
1254	Monodentate nitrate	[47]
1452	Symmetrical surface nitrate	[47]
1648	Surface undissociated water	[45,46]
1713	Free nitrate	[48]

In conclusion, we develop a facile method to prepare La-doped ZnO photocatalysts. Combined with DFT calculations, ESR spectra and *in situ* FTIR spectra, the conversion pathway of photocatalytic NO oxidation and mechanism of toxic intermediate inhibition on La-ZnO have been elaborated. The introduction of La^{3+} induce the redistribution of charge carriers in La-ZnO, which promote the production of $^{\bullet}O_2^-$ and lead to the formation of V_{Zn} for the enhanced generation of $^{\bullet}OH$, contributing to the complete oxidation of NO to nitrate. This work realizes the efficient photocatalytic NO removal and suppressed NO_2 generation simultaneously for efficient and safe air purification.

Acknowledgments

This work was supported by the National Natural Science Foundation of China (Nos. 21822601, 21777011 and 21501016), the Innovative Research Team of Chongqing (No. yjscxx2019-101-62), the Natural Science Foundation of Chongqing (No. cstc2017jcyjBX0052), and the Plan for "National Youth Talents" of the Organization Department of the Central Committee. The authors also acknowledge AM-HPC in Suzhou, China for computational support.

Appendix A. Supplementary data

Supplementary material related to this article can be found, in the online version, at doi:https://doi.org/10.1016/j.cclet.2019.09.033.

References

[1] L.S.R. Brickus, J.N. Cardoso, F.R.D. Neto, et al., Environ. Sci. Technol. 32 (1998) 3485–3490.
[2] M.X. Ran, P. Chen, J.R. Li, et al., Chin. Chem. Lett. 30 (2019) 875–880.
[3] S.C. Yan, R. Xu, J.L. Hu, et al., Environ. Sci. Technol. 47 (2013) 11562–11568.
[4] K.C. Taylor, Catal. Rev. 35 (1993) 475–481.
[5] F. Dong, Z.Y. Wang, Y.H. Li, et al., Environ. Sci. Technol. 48 (2014) 10345–10353.
[6] Y. Huang, P.G. Wang, Z.Y. Wang, et al., Appl. Catal. B 240 (2019) 122–131.
[7] Z.Y. Wang, Y. Huang, M.J. Chen, et al., ACS Appl. Mater. Interfaces 11 (2019) 10651–10662.
[8] M.J. Chen, Y. Huang, J. Yao, et al., Appl. Surf. Sci. 430 (2018) 137–144.
[9] Y.F. Lu, Y. Huang, J.J. Cao, et al., J. Mater. Chem. A: Mater. Energy Sustain. 7 (2019) 15782–15793.
[10] I. Heo, M.K. Kim, S. Sung, et al., Environ. Sci. Technol. 47 (2013) 3657–3664.
[11] Q.B. Guo, T.H. Sun, Y.L. Wang, et al., Environ. Sci. Technol. 47 (2013) 9514–9522.
[12] W.S. Epling, L.E. Campbell, A. Yezerets, et al., Catal. Rev. 46 (2004) 163–245.
[13] K.C.H. wan, Q. Gongshin, D. Kevin, et al., Science 327 (2010) 1624–1627.
[14] Z.H. Ai, W.K. Ho, S.C. Lee, et al., Environ. Sci. Technol. 43 (2009) 4143–4150.
[15] Y. Huang, W.K. Ho, S.C. Lee, et al., Langmuir 24 (2008) 3510–3516.
[16] G.Q. Zhu, S.P. Li, J.Z. Gao, et al., Appl. Surf. Sci. 493 (2019) 913–925.
[17] J.Y. Li, P. Yan, K. Li, et al., J. Mater. Chem. A: Mater. Energy Sustain. 7 (2019) 17014–17021.
[18] W. Cui, J.Y. Li, F. Dong, et al., Environ. Sci. Technol. 51 (2017) 10682–10690.
[19] X. Li, T. Chen, H. Lin, et al., Sci. Bull. (Beijing) 63 (2018) 219–227.
[20] B. Dong, T. Liu, C. Li, et al., Chin. Chem. Lett. 29 (2018) 671–680.
[21] M. Green, A.T. Tran, et al., Int. J. Green Nanotechnol. Mater. Sci. Eng. 1 (2019) 48–59.
[22] H.J. Yu, Y.F. Zhao, C. Zhou, et al., J. Mater. Chem. A: Mater. Energy Sustain. 2 (2014) 3344–3351.
[23] S. Luan, D. Qu, L. An, et al., Sci. Bull. (Beijing) 63 (2018) 683–690.
[24] H. Li, H. Shang, X. Cao, et al., Environ. Sci. Technol. 52 (2018) 8659–8665.
[25] W.C. Wang, G.M. Cool, N. Kapur, et al., Science 337 (2012) 832–835.
[26] J.Y. Li, W. Cui, Y.J. Sun, et al., J. Mater. Chem. A: Mater. Energy Sustain. 5 (2017) 9358–9364.
[27] Y. Wang, X.C. Wang, M. Antonietti, et al., Angew. Chem. 2 (2012) 68–89.
[28] J.L. Zhang, Y.M. Wu, M.Y. Xing, et al., Energy Environ. Sci. 3 (2010) 715–726.
[29] X.B. Chen, S.H. Shen, L.J. Guo, et al., Chem. Rev. 110 (2010) 6503–6570.
[30] J. Lasek, Y.H. Yu, J.C.S. Wu, et al., J. Photochem. Photobiol. C: Photochem. Rev. 14 (2013) 29–52.
[31] F. Dong, Z.Y. Wang, Y.H. Li, et al., Environ. Sci. Technol. 48 (2014) 10345–10353.
[32] Y. Nosaka, A.Y. Nosaka, Chem. Rev. 117 (2017) 11302–11336.
[33] M. Samadi, M. Zirak, A. Naseri, et al., Thin Solid Films 605 (2016) 2–19.
[34] M.H. Li, Y.W. Chen, T.S. Lin, et al., ACS Catal. 8 (2018) 6862–6869.
[35] J.J. Macías-Sánchez, L. Hinojosa-Reyes, A. Caballero-Quintero, et al., Photochem. Photobiol. Sci. 14 (2015) 536–542.
[36] P.W. Huo, J.Z. Li, Z.F. Ye, et al., Chin. Chem. Lett. 28 (2017) 2256–2262.
[37] N.T. Hanh, N.L.M. Tri, D.V. Thuan, et al., J. Photochem. Photobiol. A: Chem. 382 (2019)111923.
[38] S. Wang, B.C. Zhu, M.J. Liu, et al., Appl. Catal. B 243 (2019) 19–26.
[39] S.G. Ullattil, P. Periyat, B. Naufal, et al., Ind. Eng. Chem. Res. 55 (2016) 6413–6421.
[40] M. Guo, P. Diao, S.M. Gai, et al., Chin. Chem. Lett. 15 (2004) 1113–1116.
[41] V.H.T. Thi, B.K. Lee, Mater. Res. Bull. 96 (2017) 171–182.
[42] M.D. McCluskey, S.J. Jokela, J. Appl. Phys. 106 (2009) 071101.
[43] M.H. Li, Y.W. Chen, X.Y. Liu, et al., ACS Catal. 6 (2015) 115–122.
[44] K. Hadjiivanov, H. Knözinger, Phys. Chem. Chem. Phys. 2 (2000) 2803–2806.
[45] J.C.S. Wu, Y.T. Cheng, J. Catal. 237 (2006) 393–404.
[46] Q. Wu, R.V.D. Krol, J. Am. Chem. Soc. 134 (2012) 9369–9375.
[47] K. Hadjiivanov, V. Bushev, M. Kantcheva, et al., Langmuir 10 (1994) 464–471.
[48] T.J. Toops, D.B. Smith, W.P. Partridge, et al., Appl. Catal. B 58 (2005) 245–254.
[49] W. Cui, L. Chen, J. Li, et al., Appl. Catal. B 253 (2019) 293–299.
[50] X. Li, W. Zhang, W. Cui, et al., Chem. Eng. J. 370 (2019) 1366–1375.